Shared spatial selectivity in early visual cortex and face-selective brain regions

Anisa Y. Morsi[1], Hugo T. Chow-Wing-Bom[1,2], D. Samuel Schwarzkopf[3], Valérie Goffaux[4,5], Tessa M. Dekker[1,2], & John A. Greenwood[1]

[1]Experimental Psychology, University College London, UK

[2]Institute of Ophthalmology, University College London, UK

[3]School of Optometry & Vision Science, University of Auckland, New Zealand

[4]Psychological Sciences Research Institute, UCLouvain, Belgium

[5]Institute of Neuroscience, UCLouvain, Belgium

Corresponding author: Anisa Y. Morsi

Email: annie.morsi.18@ucl.ac.uk

Postal address: 26 Bedford Way, London WC1H 0AP

Abstract

Face recognition is widely considered to be “special”, involving dedicated brain regions with unique patterns of selectivity. This contrasts with increasing evidence for common patterns of ‘visuospatial coding’, where even high-level category-selective areas share the spatial properties of earlier brain regions. Here we examined whether the retinotopic properties of face-selective areas vary around the visual field in a similar fashion to those of early visual cortex, and whether these spatial properties could explain variations in face perception around the visual field. We carried out retinotopic mapping of early (V1-V3) and face-selective cortical regions (OFA, pFus, mFus) using large-field bars of faces (21° eccentricity), with spatial selectivity measured via population receptive field (pRF) analysis. While pRFs were considerably larger in face-selective regions than in V1-V3, their size did not vary consistently either across areas or in line with behavioural anisotropies. However, both early cortex and face-selective areas show a greater number of pRFs and a concomitant increase in visual field coverage along the horizontal vs. vertical meridian and in the lower vs. upper field. Variations in our face-recognition abilities around the visual field could thus be driven by these differences in sampling. We also show that pRF numbers (and subsequent coverage) in mFus were typically greater for upright than inverted faces, suggesting these properties could similarly support the perceptual advantage for upright faces, at least in part. The commonality of these variations in visual field sampling between face-selective cortex and earlier visual regions further support a hierarchical model whereby the spatial selectivity of higher-level areas is built upon the selectivity of lower regions, even for specialised face processing.

Keywords

Retinotopic organisation, visual cortex, face perception, spatial vision, specialisation.

Introduction

Face recognition is both crucial to our everyday lives and exceedingly complex for the visual system to achieve (Bruce & Young, 1986). The importance of this process is illustrated through extensive evidence that faces have a 'special' status in the visual system relative to other object types, with processing that occurs in distinct brain regions (Kanwisher et al., 1997; Grill-Spector et al., 2017) via unique cognitive mechanisms, including a disproportionate disruption from inversion (Yin, 1969; Rossion & Gauthier, 2002). This uniqueness seems at odds with a broader drive for 'canonical computations' within the brain (Miller, 2016), particularly given increasing evidence for a common pattern of 'visuospatial coding', where high-level category-selective brain regions retain at least some degree of the retinotopic organisation seen in lower-level areas (Groen et al., 2022). Here we used population receptive field (pRF) mapping (Dumoulin & Wandell, 2008) to examine whether the retinotopic properties of face-selective brain regions show biases towards specific visual field locations, similar to the anisotropies of early visual cortex, and whether these properties could explain variations in face perception around the visual field.

A ubiquitous feature of our visual abilities is their variation according to the angular location around fixation. These variations affect abilities ranging from acuity and contrast sensitivity to crowding, with the best performance along the horizontal vs. the vertical meridian (horizontal-vertical anisotropy) and in the lower vs. upper visual field (upper-lower anisotropy; Carrasco et al., 2001; Westheimer, 2003; Abrams et al., 2012; Greenwood et al., 2017; Himmelberg et al., 2020; Barbot et al., 2021). Despite early reports that face perception varied around the visual field in a distinct or wholly idiosyncratic fashion (Afraz et al., 2010; Quek & Finkbeiner, 2014; Schmidtmann et al., 2015; Quek & Finkbeiner, 2016; Visconti di Oleggio Castello et al., 2018), recent behavioural research has revealed a systematic pattern of variations similar to those of low-level vision, with better resolution for judging face gender along the horizontal vs. vertical meridian and in the lower vs. upper field (Morsi et al., 2024) and larger inversion effects on the horizontal vs. vertical meridian (Roux-Sibilon et al., 2023). At present, it is not known whether these variations in face perception reflect variations

in the sensitivity of face-selective mechanisms, or an inherited pattern of sensitivity from earlier visual processes.

Increasing evidence suggests that the low-level performance anisotropies for processes like acuity derive from variations in the retinotopic properties of early visual cortex. In areas V1-V3, smaller pRFs have been found along the horizontal (vs. vertical) meridian (Silson et al., 2018; Silva et al., 2018), though an upper-lower anisotropy in pRF size is less consistent (Silva et al., 2018; Himmelberg, Tuncok, et al., 2023). V1 also has a larger surface area and a corresponding increase in the number of pRFs along both the horizontal vs. the vertical meridian and in the lower vs. upper field (Amano et al., 2009; Himmelberg, Tuncok, et al., 2023). Variations in low-level vision can therefore be linked to differential sampling of the visual field within early visual cortex.

Faces are processed using a network of specialised brain regions, including the occipital face area (OFA) and two regions of the fusiform face area (FFA), known as pFus and mFus (Grill-Spector et al., 2017; Haxby et al., 2000). These areas show high category-selectivity towards faces relative to other objects, along with a *featural* selectivity for upright over inverted faces (Kanwisher et al., 1997; Grill-Spector et al., 2017). Although these category-selective areas were initially argued to be invariant to the spatial location of objects in the visual field (Tanaka, 1996), more recent population receptive field analyses reveal some degree of *spatial* selectivity in the form of retinotopic organisation. Though pRFs in face-selective brain regions are many times larger than those of V1 (Kay et al., 2015), they show the expected increase in size with distance from fixation and an over-representation of positions near the fovea (Kay et al., 2015; Finzi et al., 2021; Silson et al., 2022), as occurs in earlier areas (Amano et al., 2009). Oddly however, *larger* pRFs and reduced visual field coverage in face-selective areas have been linked to better face recognition, with larger pRFs found for upright vs. inverted faces (Witthoft et al., 2016; Poltoratski et al., 2021). This divergence from the more typical characteristics of retinotopy mentioned above, where smaller receptive fields are associated with better low-level acuity (Duncan & Boynton, 2003; Silva et al., 2021), suggests that the relationship between the spatial selectivity

of face-selective areas and face perception could differ from broader processes in the visual system.

The above picture highlights a puzzling dissociation between low- and high-level vision. On the one hand, face-selective regions may have distinct retinotopic properties that diverge from the variations in our visual abilities. On the other, the visual system may encode objects within a common spatial framework, with similar retinotopic characteristics shared across the hierarchy (Groen et al., 2022) in a way that drives our vision. Here we ask firstly whether the retinotopic organisation of face-selective areas is distinct from that of early visual cortex, and secondly whether the retinotopic properties of face-selective cortex could drive our face-recognition abilities. To investigate these questions, we carried out wide-field retinotopic mapping of early visual areas V1-V3 and three regions of the core face processing network: the occipital face area (OFA), and the posterior (pFus) and medial (mFus) fusiform gyrus which comprise the FFA. The spatial selectivity of each brain region was assessed via three retinotopic properties: pRF size, pRF number (quantity), and visual field coverage. We specifically asked whether these measures varied according to visual field location (*spatial selectivity*) and when the mapping was performed with upright vs. inverted faces (*featural selectivity*).

If face-selective areas share their spatial selectivity with earlier regions, there should be some combination of smaller pRFs, a greater *number* of pRFs, and/or *increased visual field coverage* along the horizontal vs. vertical meridian and in the lower vs. upper field in both early visual cortex and face-selective regions, matching the above observations in both early cortex and visual performance. Alternatively, if the spatial selectivity of face-selective regions is distinct from that of earlier areas, higher regions may show either invariant spatial properties around the visual field, or wholly distinct variations. The latter may arise if large receptive fields benefit face perception (Witthoft et al., 2016; Poltoratski et al., 2021), in which case pRFs in face-selective cortex should be *larger* along the horizontal vs. vertical meridian, in the lower vs. upper field. Given the observation of larger pRFs for upright vs. inverted faces (Poltoratski et al., 2021), we further examined whether these retinotopic properties

differed with face orientation in a consistent manner to drive both these variations in *featural selectivity* and the above variations in *spatial selectivity*.

Methods

Participants. Ten participants (six female, four male, M_{age} = 29.1 years) took part, all of whom had normal or corrected-to-normal vision and gave written informed consent. The experiment was approved by the Research Ethics Committee for Experimental Psychology at University College London.

Apparatus. Functional and anatomical scans were obtained using a Siemens Prisma 3T MRI scanner (Siemens, Erlangen, Germany). Stimuli were displayed on a back-projection screen in the bore of the magnet using an EPSON EB-L1100U projector that had a maximum luminance of 502 cd/m^2. The projector had a refresh rate of 60 Hz and a resolution of 1920 x 1200 pixels, with stimuli displayed in the central 1200 pixels (at a physical size of 27 x 27 cm). Participants viewed the screen through a mirror attached to the head coil at a viewing distance of 34 cm, giving a maximum field of view of 43.3° (±21.65° eccentricity). Gamma correction was performed, with the grey stimulus background presented at the mean projector luminance (251 cd/m^2).

Stimuli. Stimuli were programmed using MATLAB (MathWorks, Inc) and PsychToolbox (Brainard, 1997; Pelli, 1997; Kleiner et al., 2007). 15 male and 15 female faces were selected from the Radboud Face Database (Langner et al., 2010). Images were in colour and faces had a neutral expression. To maximise face-selective activation, we sought to minimise adaptation, crowding, and repetition suppression effects (Fang et al., 2007; Henson, 2016; Kalpadakis-Smith et al., 2018), by using faces with three viewpoints according to the view of the model: front- (90°), left- (135°) and right-facing (45°). This resulted in a total of 90 face images, which had their background removed and were resized to be 332 x 450 pixels using Adobe Photoshop CS6.

While there is evidence that a wedge and ring approach to retinotopic mapping produces better goodness-of-fit in V1 compared to bar stimuli (Alvarez et al., 2015),

this approach requires eccentricity scaling to an extent that is unclear in face-selective regions. Instead we chose to use bars, which have been shown to map eccentricities outside of the fovea more accurately than wedge and ring stimuli (Linhardt et al., 2021). Bars covered the full field of view in length (43.3°; Figure 1A). To improve the visibility of faces in the periphery and to improve pRF fitting by maximally activating differently sized pRFs (both smaller pRFs near the fovea and larger pRFs peripherally), three different bar thicknesses were used, covering 5.30°, 6.97° and 10.06° in width. Face size was determined by the width of the bar so that faces would fit within the bars (i.e. face sizes varied with bar sizes).

For each bar width, orientation (horizontal and vertical) and face condition (upright or inverted), five bars containing male faces and ten bars containing female faces were generated (male bars appeared less frequently). As above, each bar contained faces of different viewpoints in a pseudo-randomised manner, such that faces of one viewpoint could not appear next to a face of the same viewpoint. To further avoid adaptation/suppression effects tied to identity (Natu et al., 2016), each identity could not appear in the same bar twice. The position of the faces within the bars was shifted along the width of the bar (the x axis for vertical bars and the y axis for horizontal bars) so that they could be moved closer together along the opposite axis, reducing blank space. To further maximise the activation of face-selective regions, and to ensure even presentation of the faces within each bar, faces were moved along the length of the bar during presentation (at a speed of 92.03–107.48 deg/sec depending on the bar width and orientation). To allow this motion, bars were initially made longer than required (varying from 49.08–57.32° depending on bar width and orientation) and then cropped eight times along the longer axis, with each crop cutting out a bar of the desired length but starting at a different point at equal increments along the bar. This resulted in eight differently cropped versions of each bar, played in sequence to simulate motion. For the inverted face bars, faces were flipped along the vertical axis. The background of each bar matched the grey background of the experimental screen.

Procedure. Each run began with a blank screen for five seconds, with a central fixation cross subtending 0.95° of visual angle. Bars then stepped the screen in four directions: 0° (rightwards), 90° (upwards), 180° (leftwards) and 270° (downwards), appearing in one location per repetition time (TR), which lasted one second (Figure

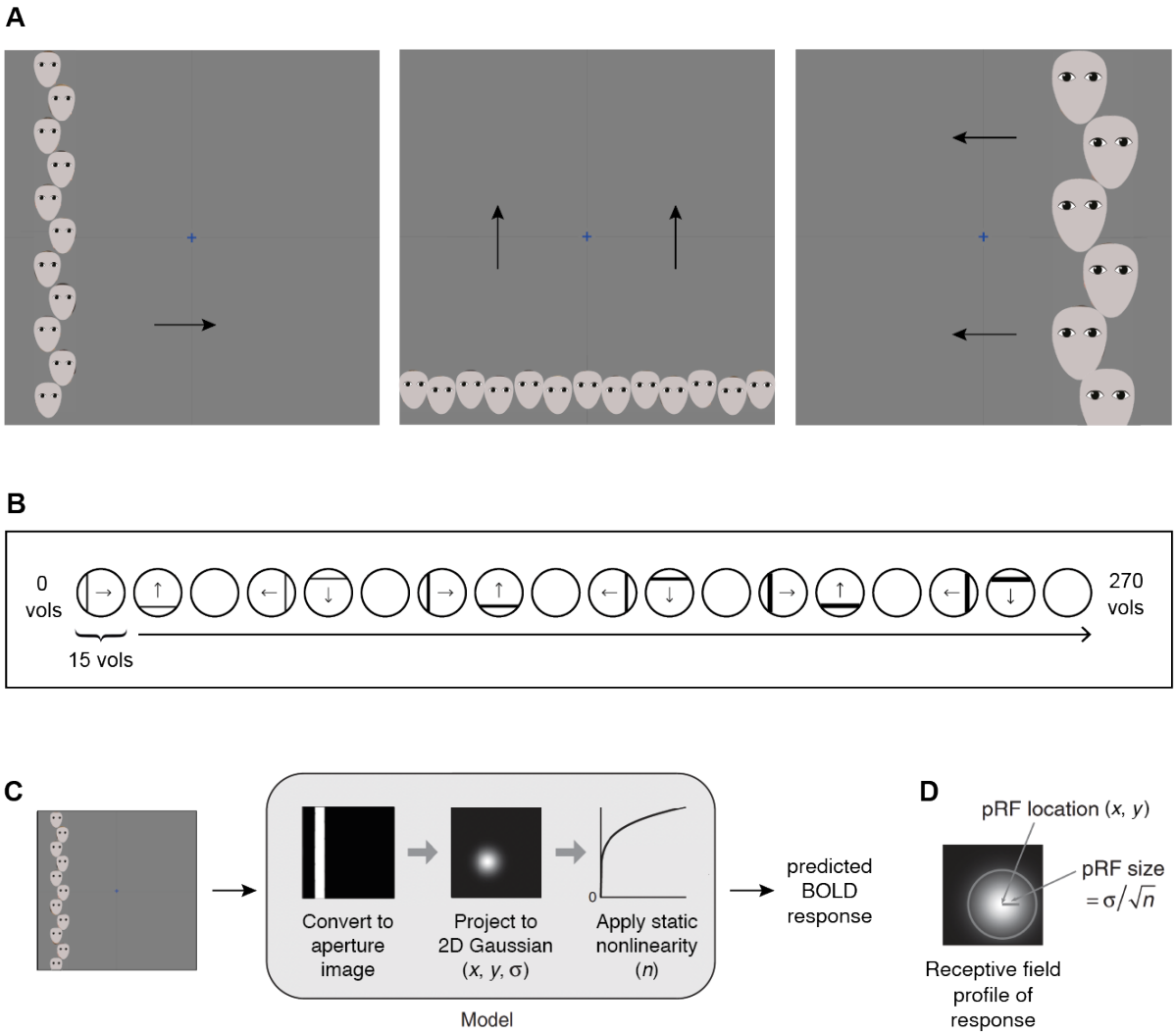

Figure 1. **A.** Examples of retinotopic mapping stimuli. A blue fixation cross appeared at the centre of the display while bars containing either male or female faces traversed the screen in one of four directions: 0° (rightwards), 90° (upwards), 180° (leftwards) and 270° (downwards). Arrows represent the direction of motion. Different bar thicknesses are shown in different panels. Bars appeared at one location per TR (one second), with various crops shown in quick succession to induce the illusion of motion. **B.** Bar conditions throughout the experiment. For illustration purposes the screen is shown as a circle, with each circle representing one sweep (15 TRs/locations) across the screen. The smallest width bars were shown first, then the medium, then the largest width. Blank periods (15 TRs) occurred after every two sweeps. Arrows represent the bars' direction of movement. **C.** pRF model. The stimulus was converted to a binary aperture image and each pRF modelled as a 2D Gaussian before a static nonlinearity was applied using a compressive spatial summation parameter. The model output is the predicted BOLD response. **D.** Definition of pRF location and size in the compressive spatial summation model. Position is determined by *x* and *y* coordinates, while size is the standard deviation (σ) divided by the square root of the spatial summation exponent *n.* Figures C and D are adapted from Kay et al., (2013).

1B). Each sweep across the screen contained 15 equal steps, meaning that steps were smallest with the largest bar widths and vice versa. The number of steps was kept the same to avoid the pRF fitting being biased towards bar widths with more TRs (by contributing more to the least-squared error between data and model predictions used for model fitting). The thinnest bars were presented first (four sweeps, one per direction of motion) before moving on to the next thickness. As there were three bar thicknesses, each run had a total of 12 sweeps. Every second sweep (i.e. after 0° and 90°, then after 180° and 270°) was followed by a blank period of 15 TRs. Each run therefore comprised 275 TRs, lasting four minutes and 35 seconds.

As above, faces were moved along the length of the bar to ensure that the time-averaged bar for each TR would have contained faces in as much of the bar as possible. On each step, the bar was presented from the first to the eighth crop and then back to the first, meaning that 15 crops of each bar were shown in succession for 66.7 ms each. As such, the faces within the bars appeared to move smoothly side to side (horizontal bars) or up and down (vertical bars) at each location.

Most bars contained female faces, while bars consisting of male faces occurred with 0.075 probability. Participants were instructed to maintain fixation on a fixation cross at the screen centre, whilst performing two tasks. To ensure that attention was directed towards the bars whilst also encouraging fixation, participants were required to respond either when a bar containing male faces appeared, or when the fixation cross changed from blue to purple (0.002 probability, and lasting 0.2 seconds). Responses were recorded via a button box. Participants did not receive feedback, however key presses were monitored throughout the experiment to ensure that participants were engaging with the task. Upright and inverted runs were interleaved to avoid effects like fatigue disproportionately affecting one condition.

Localisation of face-selective ROIs. To identify face-selective regions of interest (ROIs), a functional localiser was run in the same scan session. As most previous studies investigating FFA activity displayed stimuli to the central 6-8° of the visual field, face localisers tend to use small, foveal stimuli. We were concerned that a similar approach would bias our localisation of face-selective regions towards voxels

with a preference for foveal stimuli, which would exaggerate the extent of the foveal bias within face-selective regions. As a result we developed a novel localiser which presented faces and objects in both foveal and peripheral locations, at a variety of sizes. Images of faces, hands and instruments were displayed using the same maximum eccentricity (21.65°) as the retinotopic mapping stimuli, so images covered a 43.3° field of view. To maximise both foveal and peripheral stimulation, two configurations of stimuli were used: large, single images centred on the fovea, and smaller images which were tiled across the screen in a nine-by-nine grid. Similar to existing approaches (Stigliani et al., 2015), faces, hands and instruments were shown in separate blocks lasting ten seconds each, interspersed by baseline (blank) periods. Within each block there were 20 stimuli displayed for 500 ms each. Single and tiled configurations were presented in the same run, in different blocks. Each run consisted of 51 blocks, lasting eight minutes and 35 seconds. Participants were instructed to maintain fixation and press a button when a phase-scrambled image appeared. Each participant completed two runs.

To identify face-selective brain regions we contrasted blood-oxygen-level-dependent (BOLD) responses in response to faces against the other object categories (Kanwisher et al., 1997; Weiner & Grill-Spector, 2010), combining both single and tiled versions (single and tiled faces > single and tiled hands, plus single and tiled instruments) using a general linear model (GLM) performed in SPM12 (Ashburner & Friston, 2014). Statistical contrasts were carried out using a threshold of $t \geq 2$, which was chosen to help maximise the number of pRFs remaining for further analyses after filtering by

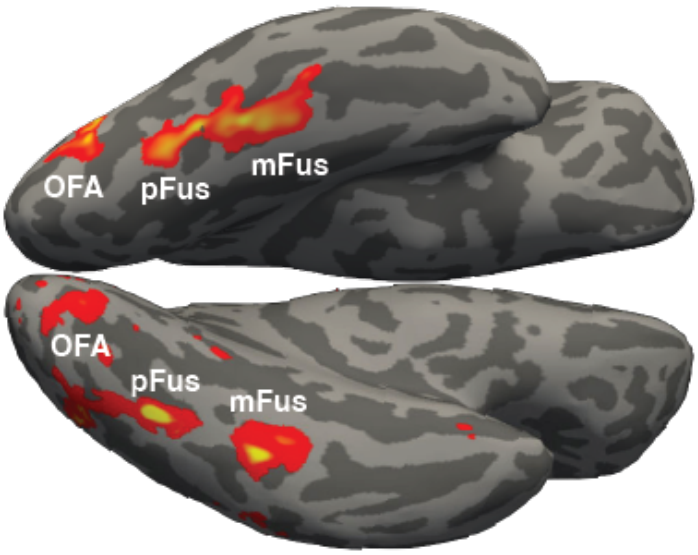

Figure 2. The location of face-selective ROIs on the ventral surface of one participant's brain.

visual field location. We defined three face-selective areas (OFA, pFus and mFus; Figure 2) in nine participants, though only two were possible to define in the remaining participant (OFA and mFus). Statistical *T* maps were surface projected using Freesurfer (Fischl, 2012) and used as a visual guide during the delineation of face-selective ROIs. Large areas were initially drawn manually, before an automatic process defined the ROI by identifying the vertex with the peak *T* statistic in each region, along with any neighbouring vertices that were above the chosen *T* threshold ($t \geq 2$).

MRI data acquisition. A 64-channel head coil was used with the 3T scanner, with cushions placed around participants' heads in order to minimise movement. A T1-weighted anatomical magnetisation-prepared rapid acquisition with gradient echo (MPRAGE) image was acquired (TR = 2300 ms and TE = 2.98 ms, voxel size = 1 mm isotropic voxels). Functional scans were run with only the back of the head coil, leaving 42 channels. Functional T2-weighted multiband 2D echoplanar images were acquired (TR = 1000 ms, TE = 35.20 ms, voxel size = 2 mm isotropic voxels, 48 slices, flip angle = 60°, acceleration factor = 4). Each functional scan contained 270 volumes. A short 30 second localiser was carried out before the functional scans and again before the anatomical scan, after the front head coil was fitted. Fixation was monitored throughout the experiment using an Eyelink 1000, although we did not record fixation data.

MRI data preprocessing. For each participant, the T1 anatomical scan was automatically segmented and used to generate a 3D representation of the cortical surface using Freesurfer (Dale et al., 1999; Fischl et al., 1999; Fischl, 2012). Functional images were B0 distortion corrected and motion corrected using AFNI software (Cox, 1996). An alignment volume was created by finding the volume with the fewest voxel outliers across all runs, which all functional volumes were then aligned to. Using Freesurfer (Fischl, 2012), the alignment volume was co-registered to the structural image, and surface projection was performed.

pRF fitting. The four runs were concatenated and pRF analyses carried out using the SamSrf 9.4 MATLAB toolbox (Schwarzkopf, 2022). A compressive spatial summation (CSS) model (Kay et al., 2013) was used within SamSrf 9.4 (Figure 1C),

where each pRF was estimated as a two-dimensional Gaussian with a compressive non-linearity that was subsequently applied. This approach estimates pRF properties with a higher goodness-of-fit (R^2) compared to a linear pRF model, particularly in higher visual areas where responses to visual stimuli sum in a subadditive rather than linear manner (Figure S1; Kay et al., 2013). The CSS model fitting involved four free parameters: x and y (the position of the pRF within the visual field, with x_0 and y_0 denoting the centre), σ (the standard deviation or spatial spread of the pRF, in degrees of visual angle) and n (the exponent of the compressive non-linearity; Figure 1D and S3). As the compressive nonlinearity affects the spread of the receptive field profile, during analyses we defined pRF size as σ divided by the square root of the exponent n (Kay et al., 2013). Stimulus locations were fed into model fitting via stimulus apertures created for each run, which were averaged across the four runs, resulting in one set of apertures comprising 270 frames (one for each TR). Due to the motion of the bar stimuli (described above) and the averaging over time, apertures formed solid bars rather than containing space between faces (Figure 1C).

The pRF fitting involved a coarse-to-fine approach. The coarse fit was carried out using an extensive multidimensional search space comprised of 35,496 grid points, with different combinations of x, y and σ at each vertex. The parameters with the highest Pearson correlation between the predicted and observed time series were then selected. These values were used to seed the fine fit, which used the Nelder-Mead simplex-based method (Nelder & Mead, 1965) to reduce the residual sum of squares (RSS) between the predicted and observed time series, and determine optimal values for all four free parameters (x, y, σ and n).

Delineation of early visual cortex. Prior to delineation, data were smoothed using a goodness-of-fit threshold of 0.1 and a smoothing kernel of 3 mm full width half maximum (FWHM). pRF locations (x and y) were used to project colour-coded polar angle and eccentricity maps onto the cortical surface (Figure 3). Visual areas V1-V3 were delineated using an auto-delineation tool and then corrected manually using SamSrf 9.4 (Schwarzkopf, 2022). This involved using standard criteria based on reversals in polar angle (DeYoe et al., 1994; Sereno et al., 1995; Engel et al., 1997), assisted by the eccentricity maps. Regions were delineated based on the maps

generated for the upright face condition, before being checked and corrected (if needed) using the inverted maps. Higher areas were determined via localiser analyses, as above.

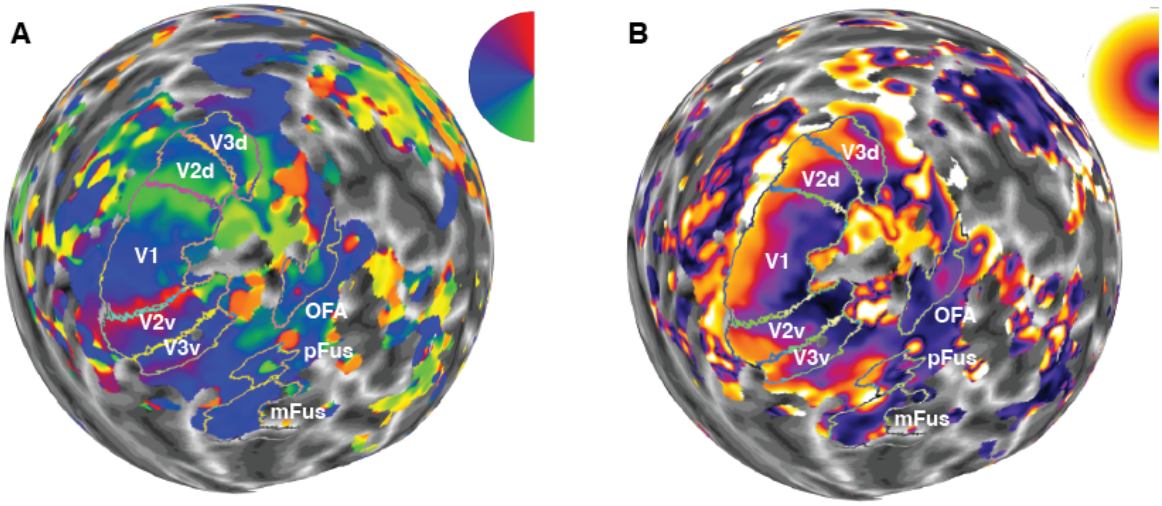

Figure 3. Retinotopic maps obtained from one participant. **A.** A polar angle map plotted on an inflated, spherical cortical surface (right hemisphere), with delineations of V1-V3 and OFA, pFus and mFus outlined. The colour wheel indicates polar angle coordinates (green for the lower visual field, blue around the horizontal meridian, red for the upper field). **B.** An eccentricity map, where purple represents central eccentricities and yellow more peripheral locations.

Vertex selection. Vertices that had beta amplitudes of less than 0.01 or greater than 3 (*z* scores), sigma values of 0, or were located perfectly at the centre (*x* and *y* of exactly 0, which is indicative of fitting errors) were removed. To avoid noisy and unreliable vertices, those with a goodness-of-fit threshold (R^2) below 0.2 were also removed. In OFA and mFus, some participants showed vertices with very low pRF size estimates (almost 0) at high eccentricities, which upon closer analysis were the result of poor fits. To avoid these less reliable estimates affecting the main pattern of results, we adjusted the R^2 threshold within certain face-selective ROIs for some participants (OFA: four participants = 0.4, mFus: one participant = 0.4, one participant = 0.3).

Location analyses. To compare pRF properties across visual field location, pRFs were filtered according to their centre position. Four wedges were defined, each including polar angle locations within ± 45° on either side of the left horizontal, right horizontal, upper vertical and lower vertical meridians. Although behavioural research

has suggested that visual field anisotropies decline at locations more than 30° away from the meridian (Abrams et al., 2012; Benson et al., 2021), fMRI studies that used a wedge-based approach have shown that asymmetries in cortical surface were similar across different wedge widths (Himmelberg, Tuncok, et al., 2023), and that anisotropies in pRF properties could be found using 45° wedges (Silva et al., 2018). In our data, patterns were generally similar regardless of whether the wedge width was 30° or 45°. As a wider wedge width of 45° considerably increased the number of pRFs remaining after filtering, we chose to use 45° wedges. For horizontal-vertical comparisons, the left and right wedges were combined to make the horizontal meridian, with the upper and lower wedges combined to make the vertical meridian.

Visual field coverage. Visual field coverage was determined by generating a Gaussian receptive field profile for each vertex based on its centre position (x,y), eccentricity and sigma (σ), and then raising the receptive field profile by the spatial summation exponent (n). This differs from prior studies where coverage has been calculated using binary circles (e.g. Witthoft et al., 2016; Poltoratski et al., 2021). Although these binary approaches incorporate the position and size ($2\sigma\sqrt{n}$) of receptive fields, they do not capture the spatial profiles of the constituent pRFs. By including the exponent, we aimed to better account for responsiveness across the spatial extent of each receptive field profile when generating estimates of coverage.

Receptive field profiles were summed across vertices to result in one coverage plot for each ROI, face orientation (upright/inverted), and participant. Because absolute values would differ based on various factors (e.g. number of vertices, sigma values, exponents applied), we normalised coverage values by dividing by their maximum value across both upright and inverted maps (for each ROI and participant separately). Coverage therefore represents the proportion of the peak response (within each ROI) at each visual field location. Coverage values were extracted from these plots according to eccentricity and polar angle location (using the wedges described above) for further analyses.

Statistical analyses. We were interested in three pRF properties: size ($\sigma\sqrt{n}$), number (the total amount of pRFs after poor-fitting vertices were removed) and visual

field coverage (the values extracted from the coverage plots). Eccentricity bin widths of 1° were used for the statistical analyses of all three properties. The eccentricity range spanned from 0.5° (to exclude the region where the fixation point appeared) up to the maximum eccentricity of 21.65°, making 21 bins in total.

Linear mixed effects models were used to investigate whether location, inversion and eccentricity could predict pRF size. Because the location of each pRF was determined by its centre, size could not be estimated if there were no pRF centres within that region. Linear mixed models can deal with these “missing” estimates by examining the linear change in pRF size with eccentricity. Separate mixed effects models were run for each ROI (V1, V2, V3, OFA, pFus and mFus). Our main analyses examined pRF size with fixed factors for visual field location (horizontal/vertical or upper/lower), eccentricity and inversion (upright/inverted), while a second set examined fixed factors for eccentricity and inversion (upright/inverted) irrespective of location. Participant was specified as a random factor for the intercept as well as for each of the fixed factors, as the slope of the relationship between pRF size and eccentricity, location and/or inversion could vary across individuals. Differences at each eccentricity were then examined using Wilcoxon signed rank tests.

Mixed effects analyses of variance (ANOVAs) were used to assess the effects of eccentricity, inversion, location and participant on pRF number and visual field coverage. Separate ANOVAs were run for each ROI (V1, V2, V3, OFA, pFus and mFus). Our main set of analyses included within-subjects fixed factors for location, eccentricity, and inversion (upright/inverted), with a second set run including data irrespective of location. In all ANOVAs, participant was entered as a between-subjects random factor. Inversion effects and location differences were then examined via t-tests or Wilcoxon signed rank tests (if sphericity or homoscedasticity assumptions were violated).

Results

We used population receptive field (pRF) mapping to compare the spatial selectivity of early visual cortex (V1-V3) with three face-selective regions of ventral

occipitotemporal cortex (OFA, pFus, mFus). Maps of the visual field coverage for each ROI are displayed in Figure 4, separately for upright and inverted faces. These coverage plots show the relative responsiveness of pRFs across the visual field, incorporating the number, size, and spatial profile of each pRF within the population of vertices that responded to each stimulus. All ROIs include some degree of coverage throughout the visual field, including the farthest eccentricities tested, though a bias towards foveal locations is also evident, seen especially through the location of pRF centres (shown as black dots). This foveal bias is particularly evident in face-selective regions. While coverage patterns are similar regardless of face orientation in early visual cortex, in mFus there is better coverage in both peripheral and central locations for upright rather than inverted faces.

We first assessed how retinotopic properties (pRF size, number, and visual field coverage) differed according to polar angle, and considered whether variations in this *spatial selectivity* follow the expected pattern of visual-field anisotropies along the horizontal vs. vertical meridian and in the upper vs. lower field. As we observed similar location-based variations in these measures for upright and inverted faces, the following sections on visual field anisotropies discuss the results for upright faces only (data for inverted faces are available in Figures S4, S5 and S6). We then examined whether variations in these retinotopic properties might also subserve the *featural selectivity* of face perception – the preference for upright rather than inverted faces.

Visual field anisotropies

pRF size

As expected, pRF size increased with eccentricity in all visual regions, with size estimates much larger in the face-selective areas than in early visual cortex (Figure 5). We first compared the horizontal and vertical meridians (Figure 5A). In early visual cortex, pRF sizes did not differ significantly along the horizontal and vertical meridians in V1 (β = 0.13 [-0.16, 0.44], p = .373) and V2 (β = -0.01 [-0.38, 0.36], p = .953), contrary to predictions. A main effect of location was however found in V3 (β = 0.79 [0.17, 1.41], p = .012), with Wilcoxon tests indicating that pRFs were significantly larger along the vertical than horizontal meridian at eccentricities around 10°, consistent with

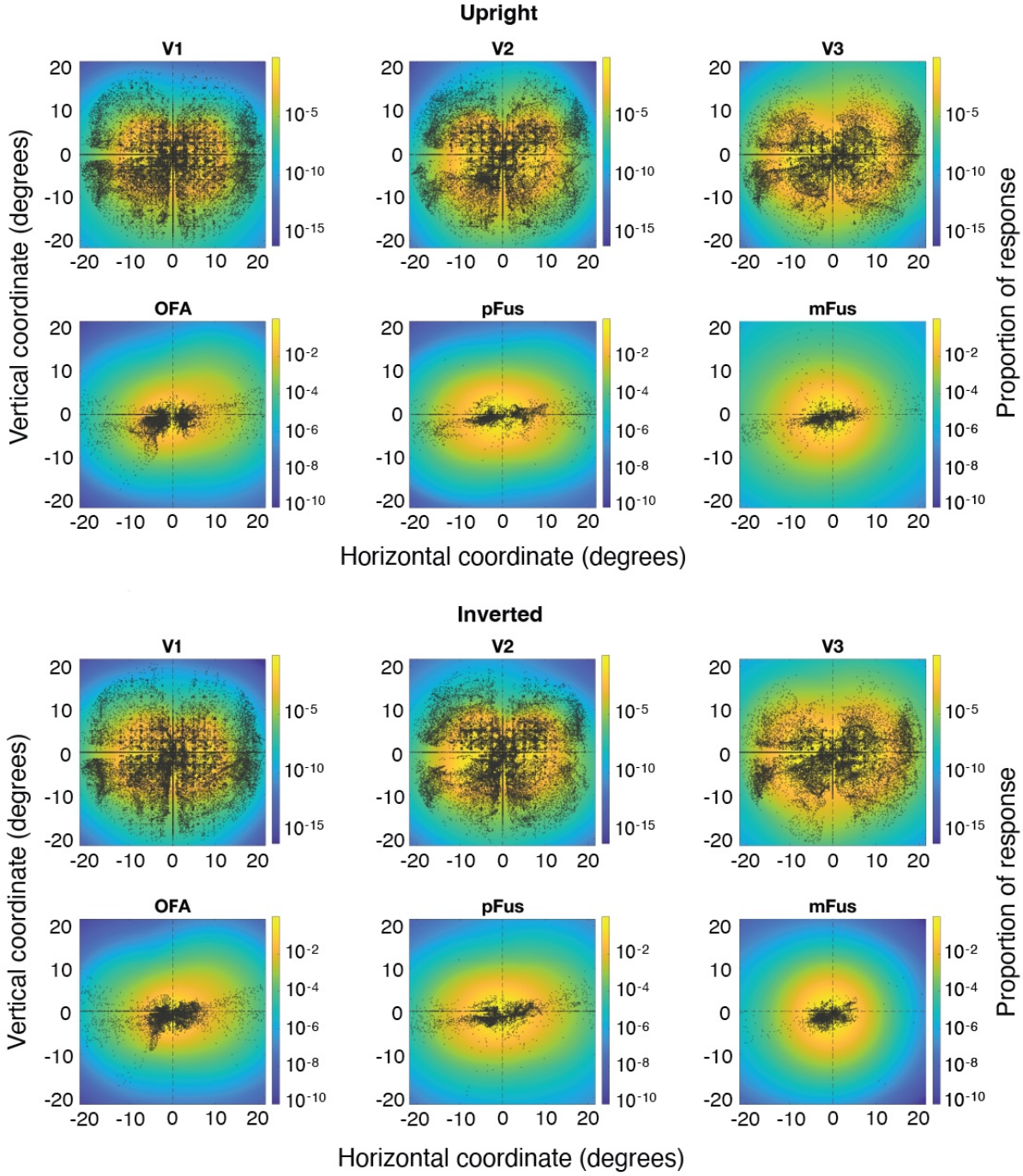

Figure 4. Mean visual field coverage for upright (top) and inverted (bottom) faces. Coordinates represent eccentricity in degrees of visual angle, with negative values for the left and positive values for the right visual field. Values were converted to log scale before plotting, for visualisation purposes (see colour bar). Dots represent pRF centres from all participants. For plots without pRF centres imposed, see Figure S3.

the pattern predicted by behavioural anisotropies. In face-selective regions, the number of pRFs in the periphery dropped markedly along the vertical meridian (to be discussed below regarding pRF number), meaning that size estimates were missing at many eccentricities. However, size estimates did not differ between the horizontal

and vertical meridian in any of these areas, shown by non-significant main effects of location in OFA (β = -0.48 [-2.05, 1.10], p = .551), pFus (β = 0.24 [-1.15, 1.63], p =

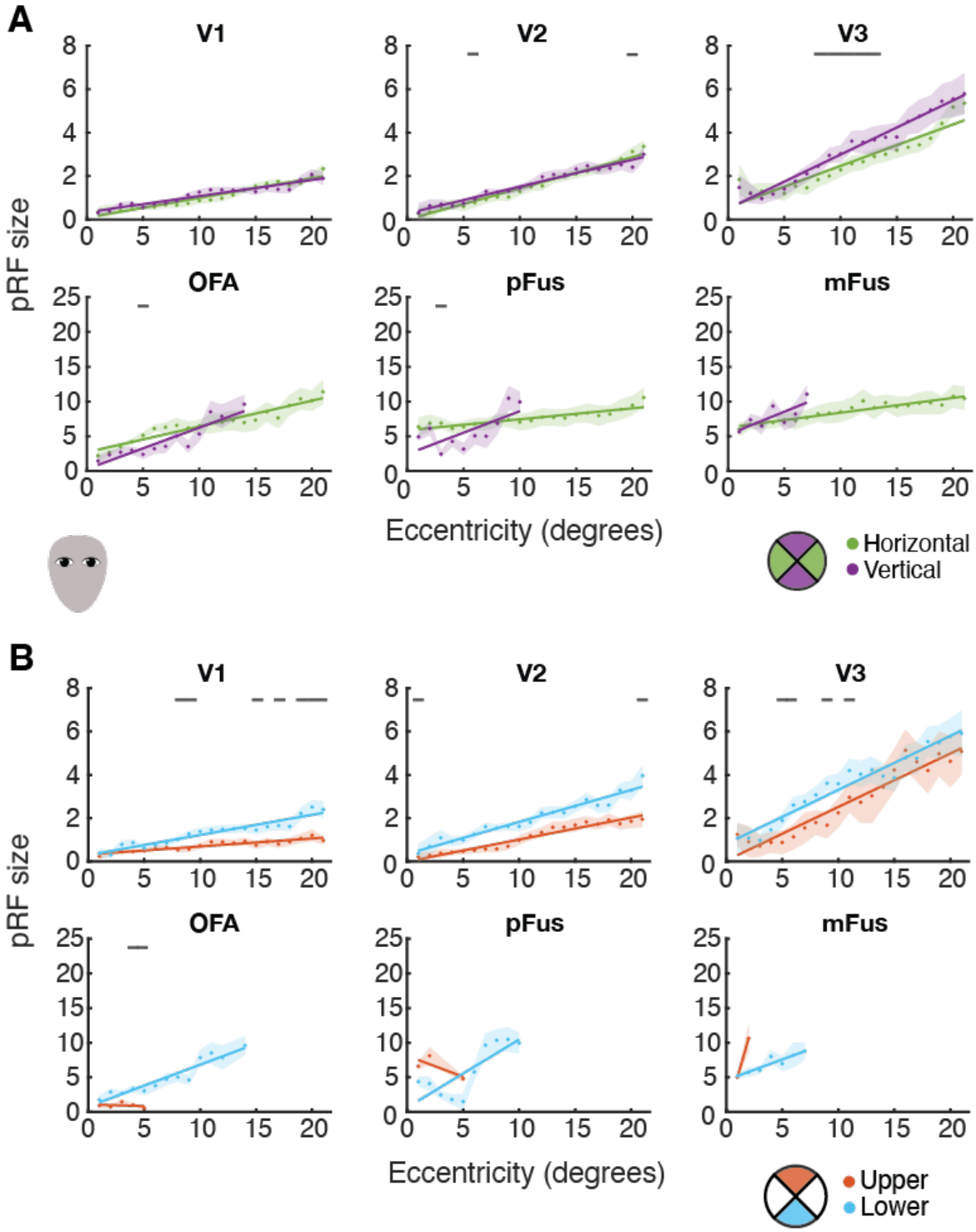

Figure 5. Mean pRF size across eccentricity along the horizontal (green) and vertical (purple) meridians **(A)** and in the upper and lower visual field **(B)**. At each eccentricity, size estimates were only plotted if they were averaged from at least five vertices. Black lines indicate significant differences according to location ($p < .05$).

.734) and mFus (β = 1.22 [-0.10, 2.54], p = .070).

Figure 5B plots the comparison of pRF sizes in the upper and lower fields. In early visual cortex, pRFs were larger in the lower than the upper field, indicated by main effects of location (V1: β = 0.66 [0.20, 1.13], p = .006; V2: β = 0.88 [0.16, 1.61], p = .017; V3: β = 0.84 [0.06, 1.62], p = .035) and significant t-test results across a range of eccentricities (Figure 5B). These significant differences run in the opposite direction to that predicted by behavioural anisotropies. In face-selective regions, there was also an effect of location in OFA (β = 2.30 [0.94, 3.67], p = .001), with pRFs again larger in the lower vs. upper field. In contrast, size estimates did not differ significantly between the upper and lower field in pFus (β = -0.72 [-4.27, 2.83], p = .689) or mFus (β = -1.72 [-3.76, 0.31], p = .096). Taken together, these findings suggest that pRF size was not consistently modulated by location in a manner following the expected behavioural anisotropies, either in early visual cortex or face-selective regions.

pRF number

We next examined the number of pRFs (defined as the number of vertices remaining after filtering by R^2, beta and sigma thresholds) in each region. As expected, the number of pRFs decreased with eccentricity in all visual areas (Figure 6). The number of pRFs was lower in face-selective areas, with more dramatic reductions in pRF number in the periphery, consistent with a magnified foveal bias in these regions compared to early visual cortex.

Figure 6A plots the differences in pRF number between the horizontal and vertical meridians. Differences were evident between the horizontal and vertical meridians in early visual cortex, with main effects of location in V1 (F(1,180) = 26.83, p < .001) and V3 (F(1,180) = 224.16, p < .001) driven by the greater number of pRFs on the horizontal meridian. Although there was no main effect of location in V2 (F(1,180) = 0.01, p = .957), all three areas show an increase in the horizontal-vertical difference with distance from the fovea, with significant interactions between location and eccentricity in each case (V1: F(20,180) = 14.64, p < .001; V2: F(20,180) = 16.54, p < .001, V3; F(20,180) = 7.94, p < .001). Wilcoxon tests showed that all three early visual areas had significantly more pRFs along the horizontal than vertical meridian in

peripheral vision, with significant differences covering a greater proportion of the visual field in V3 compared to V1 and V2.

All three face-selective regions also exhibited a greater number of pRFs along the horizontal than vertical meridian (Figure 6A), confirmed by main effects of location in each (OFA: $F(1,180) = 16.49$, $p = .003$; pFus: $F(1,160) = 15.92$, $p = .004$, mFus; $F(1,180) = 7.27$, $p = .025$). There were again interactions between location and eccentricity in all three regions (OFA: $F(20,180) = 15.86$, $p < .001$; pFus: $F(20,160) = 7.81$, $p < .001$, mFus; $F(20,180) = 6.53$, $p < .001$), with Wilcoxon tests revealing significant differences both near the fovea and in the periphery (Figure 6A). This over-representation of the horizontal meridian follows the predicted direction for behavioural anisotropies, and appears to increase throughout the visual hierarchy, with face-selective areas showing both an increased magnitude and a larger extent of the visual field where differences are evident, relative to V1-V3.

Figure 6B plots differences in the lower vs. upper field, where main effects of location in V1-V3 confirmed that there were a greater number of pRFs in the lower field, as predicted by behavioural anisotropies. Interactions between location and eccentricity were also significant (V1: $F(20,180) = 3.86$, $p < .001$; V2: $F(20,180) = 7.45$, $p < .001$, V3; $F(20,180) = 2.68$, $p < .001$), with the Wilcoxon tests showing that the upper-lower difference varied across the visual field but was generally greater towards the periphery.

As with the horizontal-vertical anisotropy, upper-lower differences in pRF number were even more pronounced in face-selective regions, with all three face-selective areas showing strikingly few pRFs in the upper field. This gave main effects of location in OFA ($F(1,180) = 7.87$, $p = .021$) and mFus ($F(1,180) = 19.06$, $p = .002$), with more pRFs in the lower than upper field, consistent with predictions. There were also interactions between location and eccentricity for OFA ($F(20,180) = 5.05$, $p < .001$) and mFus ($F(20,180) = 11.29$, $p < .001$). Although there was no main effect of location in pFus ($F(1,160) = 2.93$, $p = .125$) there was an interaction between location and eccentricity ($F(20,160) = 2.92$, $p < .001$). Wilcoxon tests showed that the upper-lower differences were more pronounced near the fovea in OFA, where there were

larger numbers of pRFs overall. Although the Wilcoxon tests did not find significant upper-lower differences in pFus and mFus, this could be related to the relatively low number of pRFs along the vertical meridian in these regions. Together, we observe

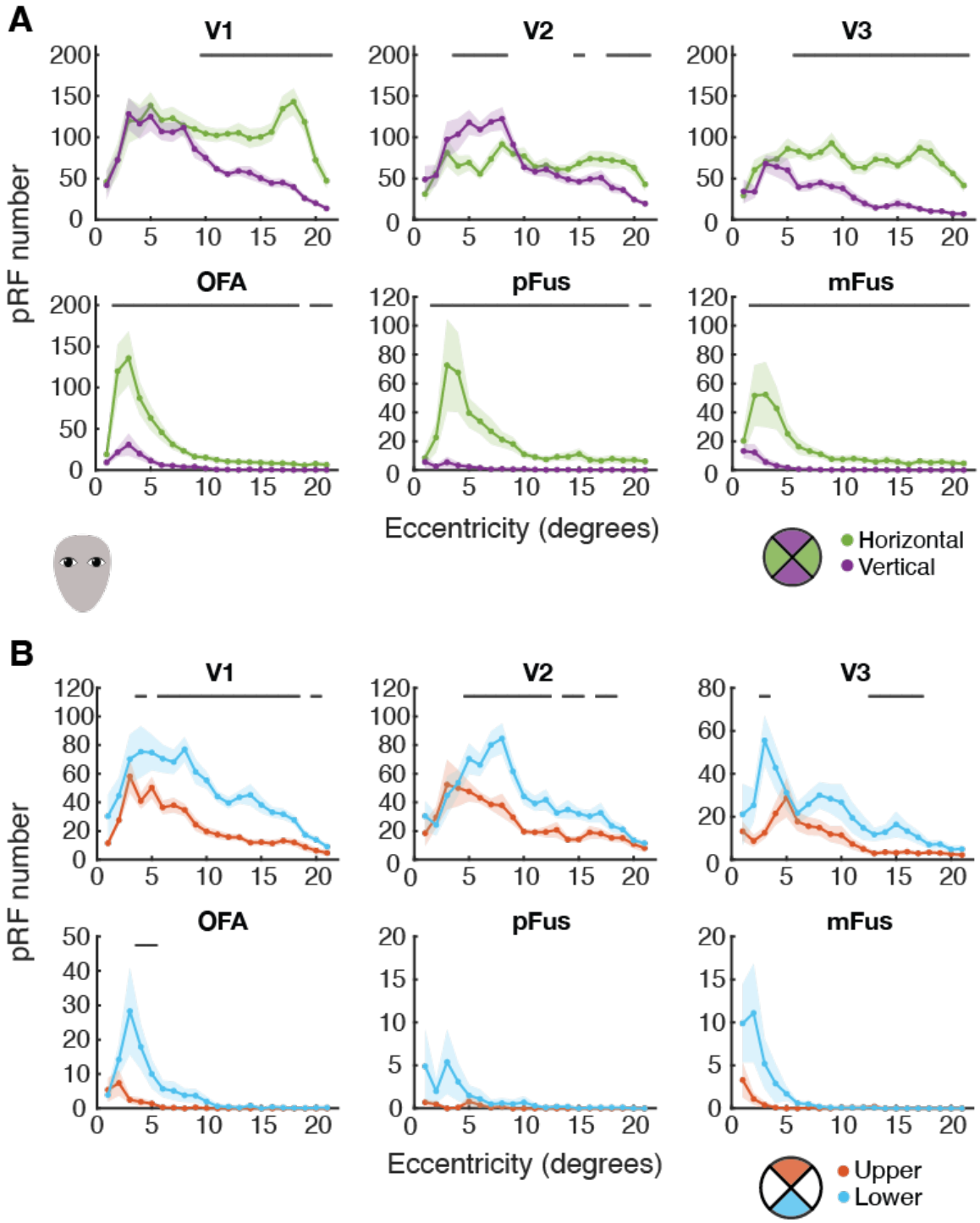

Figure 6. Mean pRF number across eccentricity along the horizontal (green) and vertical (purple) meridians **(A)** and in the upper and lower visual field **(B)**. At each eccentricity, size estimates were only plotted if they were averaged from at least five vertices. Black lines indicate significant differences according to location ($p < .05$).

more pRFs along the horizontal vs. vertical meridian and in the lower vs. upper field across both early and face-selective brain regions, in a manner consistent with behavioural anisotropies, with both horizontal-vertical and upper-lower anisotropies becoming more pronounced further up in the visual hierarchy.

Visual field coverage

To combine the above measures of pRF size and number, we next examined the variation in pRF coverage around the visual field. Figure 7 plots coverage values separated by visual field location, where a decrease in coverage with eccentricity is evident in all areas, with the most rapid drop in face-selective areas. Comparing the horizontal and vertical meridians in early visual cortex (Figure 7A), there were significant main effects of location in all three areas (V1: $F(1,180) = 8.36$, $p = .018$; V2: $F(1,180) = 9.32$, $p = .014$; V3: $F(1,180) = 46.57$, $p < .001$), driven by increased coverage along the horizontal compared to the vertical meridian, consistent with the pattern of behavioural variations. There were also significant interactions between location and eccentricity in all three regions (V1: $F(20,180) = 30.78$, $p < .001$; V2: $F(20,180) = 31.70$, $p < .001$; V3: $F(20,180) = 59.97$, $p < .001$). These interactions reflect the increased horizontal-vertical differences at more peripheral eccentricities beyond the fovea. Across early visual cortex, t-tests revealed differences at the majority of eccentricities tested, with the horizontal-vertical anisotropy becoming particularly pronounced in V3 relative to the earlier areas.

Face-selective brain regions all showed small but consistent horizontal-vertical anisotropies in visual field coverage. Main effects of location indicated that coverage was better along the horizontal vs. vertical meridian in all three face-selective areas (OFA: $F(1,180) = 11.84$, $p = .007$; pFus: $F(1,160) = 7.20$, $p = .028$; mFus: $F(1,180) = 14.94$, $p = .004$). There were interactions between location and eccentricity in OFA($F(20,180) = 3.17$, $p < .001$) and pFus ($F(20,160) = 8.67$, $p < .001$) but not in mFus ($F(20,180) = 0.27$, $p = .999$). t-tests showed that these horizontal-vertical differences were present across almost all the eccentricities in pFus, and all of them in OFA and mFus. In other words, there was a consistent horizontal-vertical difference across the visual field within face-selective cortex, in a direction consistent with behavioural anisotropies.

Upper-lower differences were similarly evident in V1-V3, with increased coverage in the lower vs. upper field, again consistent with the direction of behavioural effects. Each area accordingly gave main effects of location (V1: $F(1,180) = 25.67$, p

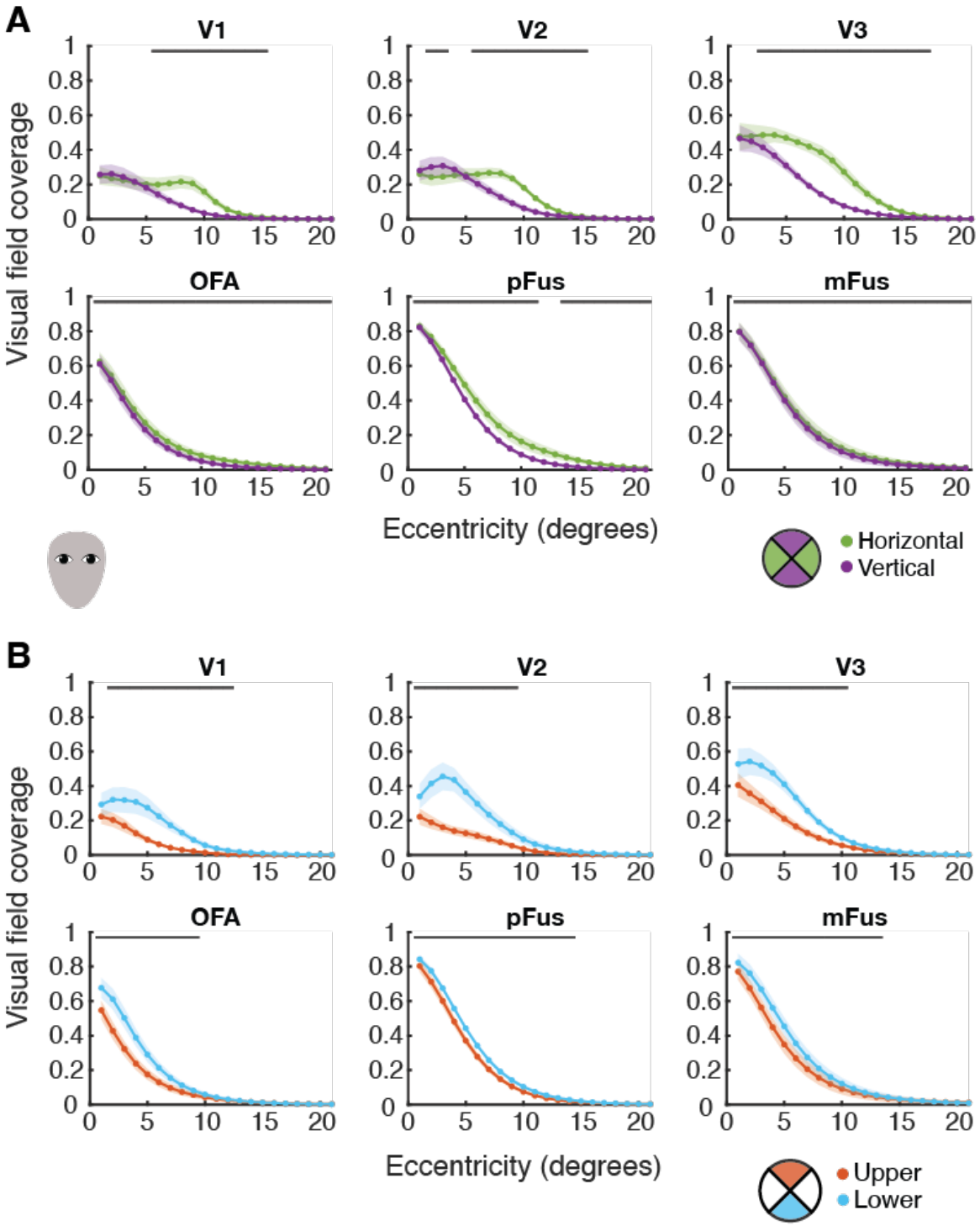

Figure 7. Mean visual field coverage across eccentricity along the horizontal (green) and vertical (purple) meridians **(A)** and in the upper and lower visual field **(B)**. At each eccentricity, size estimates were only plotted if they were averaged from at least five vertices. Black lines indicate significant differences according to location ($p < .05$).

< .001; V2: $F(1,180) = 31.87$, $p < .001$; V3: $F(1,180) = 19.72$, $p = .002$). There were also significant interactions between location and eccentricity in all three regions (V1: $F(20,180) = 30.79$, $p < .001$; V2: $F(20,180) = 51.05$, $p < .001$; V3: $F(20,180) = 32.37$, $p < .001$). t-tests confirmed the presence of significant upper-lower differences at eccentricities below 10°, with values collapsing together at higher eccentricities. Face-selective regions also had greater visual field coverage in the lower vs. upper field, shown by main effects of location (OFA: $F(1,180) = 16.09$, $p = .003$; pFus: $F(1,160) = 10.32$, $p = .012$; mFus: $F(1,180) = 24.80$, $p < .001$). Like early visual cortex, there were also interactions between location and eccentricity (OFA: $F(20,180) = 41.28$, $p < .001$; pFus: $F(20,160) = 13.21$, $p < .001$; mFus: $F(20,180) = 18.49$, $p < .001$), with t-tests again revealing upper-lower differences at eccentricities below 10-15° but not beyond. Although upper-lower differences were smaller in magnitude in face-selective regions compared to V1-V3, they were nonetheless consistently present.

In sum, coverage was consistently higher along the horizontal than vertical meridian and in the lower than upper field in both early visual cortex and face-selective areas. Together with the variations in pRF number discussed above, this suggests that low- and high-level visual areas share common anisotropies in visual field sampling, though the effect of pRF size is more variable and thus less likely to explain behavioural anisotropies.

Inversion

We show above that the spatial properties of both early and face-selective cortex vary in a manner consistent with behavioural anisotropies. Our secondary aim was to examine whether pRF size, number and coverage would also vary with face inversion in a manner that could drive the advantage for upright over inverted face recognition (Figure 8). Participants performed a gender recognition task during scans, which revealed a clear difference in performance for upright faces (Figure S8), replicating the well-established inversion effect and demonstrating that our task was sufficient to engage face-selective processes. This was unlikely to affect fixation, with performance on the fixation task equivalent in the two conditions (Figure S9). Turning to the pRF properties, pRF size increased with eccentricity in all regions at a similar

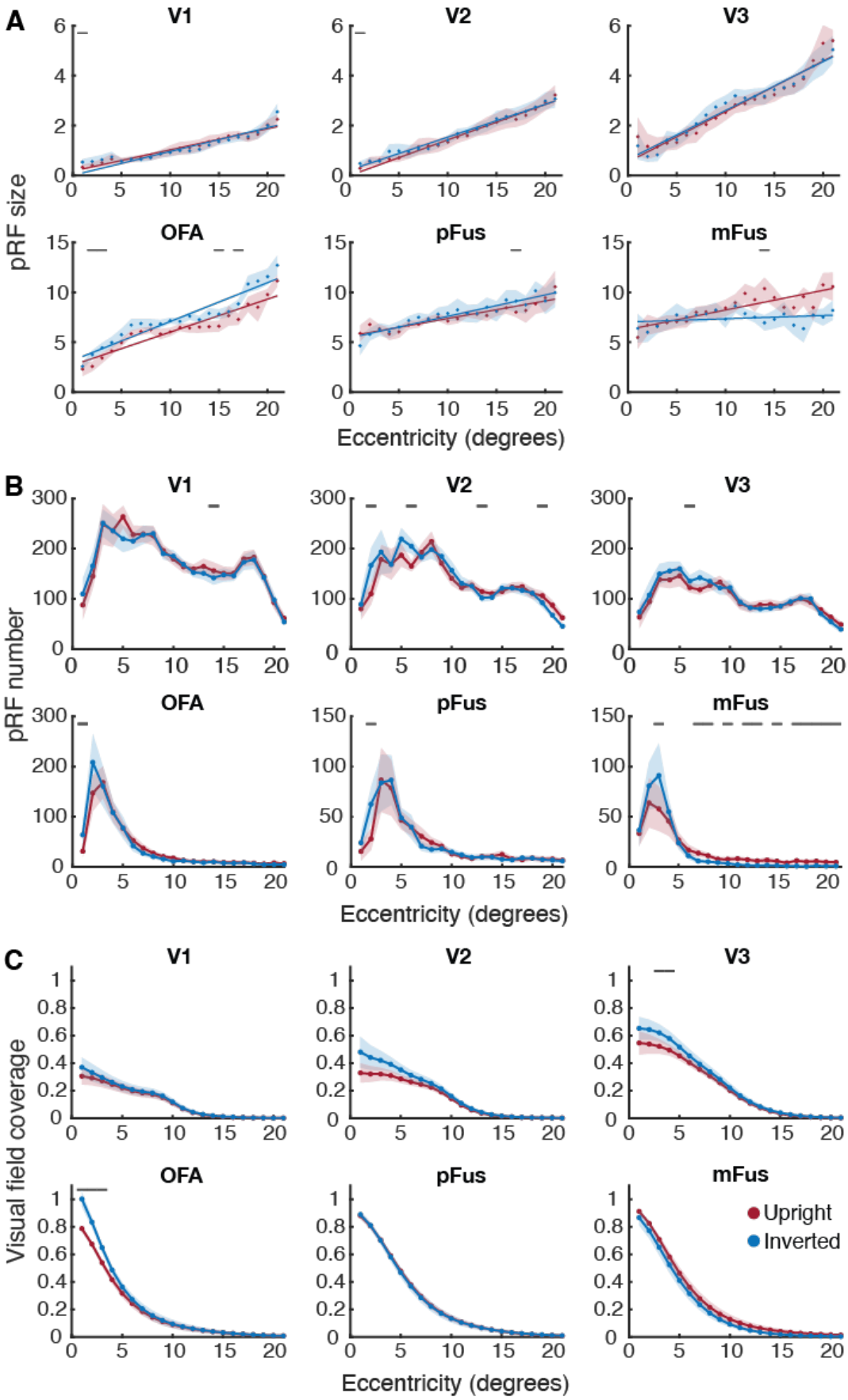

Figure 8. Mean pRF size **(A)**, pRF number **(B)** and visual field coverage **(C)** across eccentricity for upright (red) and inverted (blue) faces. At each eccentricity, size estimates were only plotted if they were averaged from at least five vertices. Black lines indicate significant differences according to face inversion ($p < .05$).

rate for both upright and inverted faces. pRF number similarly decreased with eccentricity at around the same rate for both conditions. Visual field coverage consequently decreased with eccentricity at around the same rate regardless of face orientation. In early visual cortex, there were no main effects of inversion for any of the pRF properties, as one would expect given the lack of selectivity for face orientation (Figure S10). Consequently, the following results will focus on the face-selective regions.

Previous work has reported larger pRFs for upright compared to inverted faces within the FFA (but not OFA; Poltoratski et al., 2021). Interestingly, within OFA we found larger pRFs for *inverted* than upright faces (Figure 8A), with a significant main effect of inversion (β = 0.97 [0.32, 1.61], p = .003). This difference disappeared in pFus, where pRF size was similar regardless of inversion (β = 0.32 [-0.46, 1.11], p = .416). While mFus showed small differences in locations near the fovea, there was a trend towards pRFs then becoming larger in the periphery for upright compared to inverted faces (i.e. the opposite pattern to that observed in OFA). The main effect of inversion was nonetheless non-significant (β = -0.58 [-2.45, 1.28], p = .538), with Wilcoxon tests uncovering only sporadically significant differences according to inversion within the three areas. As with the location variations discussed above, we conclude that pRF size was not modulated by inversion in a consistent manner.

For pRF number (Figure 8B), there were no main effects of inversion in any of the face-selective regions (OFA: $F(1,180) = 0.24$, $p = .634$; pFus: $F(1,160) = 2.48$, $p = .154$; mFus: $F(1,180) = 0.53$, $p = .484$). However, there were significant interactions between inversion and eccentricity in all three areas (OFA: $F(20,180) = 2.69$, $p < .001$; pFus: $F(20,160) = 1.97$, $p = .011$; mFus: $F(20,180) = 1.72$, $p = .034$). While Wilcoxon tests did not find consistent upright-inverted differences in OFA and pFus, in mFus there were significantly more pRFs for upright vs. inverted faces over the majority of eccentricities outside of the fovea. In simpler terms the distribution of pRFs across the visual field varied according to inversion in mFus, with more pRFs found in the periphery in response to upright than inverted faces.

Finally, estimates of visual field coverage (Figure 8C) were higher near the fovea for inverted vs. upright faces in OFA, with slightly better coverage across the visual field for upright vs. inverted faces in mFus. However, there were no main effects of inversion (OFA: $F(1,180) = 0.02$, $p = .884$; pFus: $F(1,160) = 0.13$, $p = .731$; mFus: $F(1,180) = 2.18$, $p = .174$), nor interactions between inversion and eccentricity (OFA: $F(20,180) = 0.97$, $p = .496$; pFus: $F(20,160) = 0.31$, $p = .998$; mFus: $F(20,180) = 1.00$, $p = .460$), indicating that visual field coverage within the face-selective regions did not significantly differ for upright and inverted faces. Therefore we do not see evidence that coverage could reliably drive differences in performance with upright vs. inverted faces, nor do pRF sizes vary consistently across these conditions, though variations in the number of pRFs sensitive to these stimuli in mFus could do so.

Discussion

Here we investigated the spatial selectivity of face-selective cortex (OFA, pFus and mFus) and its relation to that of earlier retinotopic areas. In all of these visual areas, we observe a greater *number* of population receptive fields (pRFs) and better *visual field coverage* along the horizontal vs. vertical meridian and in the lower vs. upper field in both early visual cortex (V1-V3). This demonstrates a common pattern of spatial selectivity in both early and category-selective visual areas. These variations also match behavioural anisotropies observed for both low-level visual abilities (Carrasco et al., 2001; Abrams et al., 2012; Greenwood et al., 2017; Barbot et al., 2021; Himmelberg, Winawer, et al., 2023) and higher-level face perception (Roux-Sibilon et al., 2023; Morsi et al., 2024), suggesting that variations in face perception arise due to different quantities of face-selective neurons sampling each visual field location. We also observe a reduction in pRF number in mFus for inverted relative to upright faces, suggesting that similar principles could underlie both the spatial and featural selectivity in face-selective regions. In contrast, the size of pRFs did not vary with inversion, nor did they vary in a consistent manner with visual field location in either early or face-selective regions, suggesting this property is poorly suited to explain the observed behavioural anisotropies. Variations in pRF number and visual field coverage instead offer evidence for the continuity of visuospatial coding within

the visual system, where even high-level category-selective cortex encodes objects using the same spatial framework that is established in early regions (Groen et al., 2022).

In early visual cortex, our observation of a greater number of pRFs along the horizontal than vertical meridian and in the lower vs. upper field is consistent with previous findings (Amano et al., 2009), as well as prior demonstrations of greater cortical magnification and surface area in these regions (Silva et al., 2018; Himmelberg, Tuncok, et al., 2023). Accordingly, visual field coverage was also better along the horizontal vs. vertical meridian and in the lower vs. upper field, similar to prior work (Amano et al., 2009). Here we also report clear variations in the number of pRFs – and resulting visual field coverage – in face-selective regions. OFA, pFus and mFus all had a greater number of pRFs and better visual field coverage along the horizontal than vertical meridian and in the lower vs. upper field (though the upper-lower difference in pRF number was not significant in pFus). In each case, horizontal-vertical differences were more pronounced than the upper-lower differences. This variation is, however, consistent with studies showing that the behavioural upper-lower difference is smaller in magnitude and harder to measure in both low-level vision (Barbot et al., 2021; Kurzawski et al., 2021) and for variations in the resolution of face perception (Morsi et al., 2024). Importantly, although the upper-lower anisotropy was smaller it is consistent with a general lower field bias within the visual system (Rubin et al., 1996; Fortenbaugh et al., 2015; Schmidtmann et al., 2015; Greenwood et al., 2017), showing that common hallmarks of spatial vision emerge even within specialised face processing systems.

Despite sharp reductions in pRF number in the periphery, there was at least some coverage of the visual field across all eccentricities tested (up to 21.65°) within face-selective areas (similar to V1-V3), even along the upper vertical meridian. This emphasises a role for large receptive fields that extend into peripheral vision, allowing us to recognise faces in peripheral vision (McKone, 2004; Kovacs et al., 2017; Kalpadakis-Smith et al., 2018; Roux-Sibilon et al., 2023) despite reduced numbers of neurons. The bias of face recognition towards the horizontal meridian (at the expense of the vertical) may also derive in part from people generally being of a similar height,

meaning that we typically encounter faces along the horizontal dimension (de Haas et al., 2016). Despite the clear foveal biases in face-selective regions, consistent with prior results (Kay et al., 2013; Poltoratski et al., 2021), the large receptive fields in these areas nonetheless provide coverage to support our face-recognition abilities in the periphery.

Our results do not offer support for a common pattern of variations in pRF size through the visual hierarchy. Though area V3 showed the expected horizontal-vertical difference of larger pRFs along the vertical than horizontal meridian, these differences were not observed in V1 and V2. This differs slightly from previous research, which found a horizontal-vertical difference across V1-V3 (Silva et al., 2018). We also found *larger* pRFs in the lower than upper field across early visual cortex, showing the opposite pattern to some prior work (Silson et al., 2018; Silva et al., 2018), as well as the link between smaller receptive fields and better acuity in V1 (Duncan & Boynton, 2003), though others have reported similarly little-to-no difference in pRF sizes along the vertical meridian in particular (Himmelberg, Tuncok, et al., 2023). Research also indicates that pRF size is harder to reliably measure compared to other parameters such as position, being more susceptible to change due to factors such as stimulus properties, attention, or fitting procedures (Alvarez et al., 2015; van Dijk et al., 2016). In face-selective regions, the lack of variation in pRF sizes may of course reflect the fact that pRFs in these areas are considerably larger than in V1-V3 (as is consistently found; Kay et al., 2015; Finzi et al., 2021; Poltoratski et al., 2021), meaning that they do not vary as much over location or eccentricity. Either way, the lack of reliable effects for pRF size in both early and face-selective brain regions suggests that receptive field size is not the main factor driving differences in perception across the visual field.

Our results similarly fail to reproduce the association between larger receptive fields and better face perception (Witthoft et al., 2016; Poltoratski et al., 2021), both in terms of variations around the visual field and with face inversion. We nonetheless found a clear behavioural face inversion effect, where participants were better at recognising the gender of upright compared to inverted faces (Figure S5), demonstrating the engagement of face-specific processes during our task. Prior observations of smaller pRFs for inverted vs. upright faces in the FFA (Poltoratski et

al., 2021) may instead be related to signal-to-noise variations, given the weaker beta amplitudes they observe for inverted vs. upright faces. Reduced beta amplitudes are typically associated with poorer goodness-of-fit (Schwarzkopf et al., 2014; Anderson et al., 2017), which may affect the accuracy of pRF size estimates. Indeed, lower goodness of fit has been linked specifically to smaller pRF sizes (Alvarez et al., 2015). Similarly, Hughes et al. (2019) found that reductions in pRF size could be attributed to lower stimulus visibility, with fewer voxels included in analyses due to their reduced responsivity. Instead, our results show similar beta amplitudes for upright and inverted faces in mFus (Figure S8), with differences in performance that nonetheless show the engagement of configural face processes during our task. Together these findings suggest that pRF size is not reliably modulated by face inversion.

We do however observe a greater number of pRFs for upright than inverted faces in mFus, particularly in the periphery, along with a corresponding increase in coverage for upright faces, consistent with the variation in these properties around the visual field. This suggests that changes in the number and responsiveness of face-selective neurons with face orientation could drive the differences in these abilities, at least in part. This may reflect an added inclusion of neurons selective for the configural arrangement of upright faces (Le Grand et al., 2001; Rossion, 2008) in these estimates, again consistent with the engagement of face-specific mechanisms during the pRF mapping task. However, these differences were smaller than those seen around the visual field, despite the clear behavioural face inversion effect. It is of course possible that inversion also causes differences in the firing of face-selective neurons, rather than simply differences in the number of active neurons, as previously argued (Witthoft et al., 2016; Poltoratski et al., 2021). It is nonetheless interesting to note that the horizontal-vertical and upper-lower differences in retinotopy (pRF number and coverage) were similar for upright (Figure 6Figure 7) and inverted faces (Figures S6 and S7), suggesting similar spatial selectivity within face-selective cortex regardless of the featural aspects of faces. This aligns with previous work (Morsi et al., 2024) where visual field anisotropies were comparable in magnitude for upright and inverted faces (i.e. where performance was worse overall for inverted faces, but the *differences* in performance across the visual field followed a similar pattern for upright and inverted faces). These variations, paired with the differences in pRF

number and coverage with inversion, suggest at least some commonality between variations around the visual field and with inversion.

Altogether our results demonstrate that face-selective cortex samples locations across the visual field similarly to early visual cortex, with a greater number of pRFs and better visual field coverage along the horizontal vs. vertical meridian and in the lower vs. upper field. These retinotopic variations are consistent with the behavioural anisotropies found in both low-level vision (Carrasco et al., 2001; Abrams et al., 2012; Greenwood et al., 2017; Barbot et al., 2021; Himmelberg, Winawer, et al., 2023) and for face perception (Roux-Sibilon et al., 2023; Morsi et al., 2024). In contrast, variations in pRF size are not reliably linked to behavioural anisotropies in either early or face-selective regions, although large receptive fields may be necessary to support face perception in peripheral vision given the magnified foveal bias compared to early visual cortex. Given that variations in pRF number and visual field coverage also differ according to the featural content of faces in mFus, at least some of the spatial selectivity within face-selective brain regions can be understood using common principles. The shared spatial selectivity between early visual cortex and specialised face-processing regions further evidences the common visuospatial framework used throughout the visual system.

Acknowledgements

We thank Jolien Schuurmans at UCLouvain for supplying the face images used in the functional localiser.

References

Abrams, J., Nizam, A., & Carrasco, M. (2012). Isoeccentric locations are not equivalent: the extent of the vertical meridian asymmetry. *Vision Research*, *52*(1), 70-78. https://doi.org/10.1016/j.visres.2011.10.016

Afraz, A., Pashkam, M. V., & Cavanagh, P. (2010). Spatial heterogeneity in the perception of face and form attributes. *Current Biology*, *20*(23), 2112-2116. https://doi.org/10.1016/j.cub.2010.11.017

Alvarez, I., de Haas, B., Clark, C. A., Rees, G., & Schwarzkopf, D. S. (2015). Comparing different stimulus configurations for population receptive field mapping in human fMRI. *Frontiers in Human Neuroscience*, *9*, 96. https://doi.org/10.3389/fnhum.2015.00096

Amano, K., Wandell, B. A., & Dumoulin, S. O. (2009). Visual field maps, population receptive field sizes, and visual field coverage in the human MT+ complex. *Journal of Neurophysiology*, *102*(5), 2704-2718. https://doi.org/10.1152/jn.00102.2009

Anderson, E. J., Tibber, M. S., Schwarzkopf, D. S., S., S. S., Fernandez-Egea, E., Rees, G., & Dakin, S. C. (2017). Visual Population Receptive Fields in People with Schizophrenia Have Reduced Inhibitory Surrounds. *The Journal of Neuroscience*, *37*(6), 1546-1556. https://doi.org/10.1523/jneurosci.3620-15.2016

Ashburner, J., & Friston, K. J. (2014). *SPM12 Manual.*

Barbot, A., Xue, S., & Carrasco, M. (2021). Asymmetries in visual acuity around the visual field. *Journal of Vision*, *21*(1), 2. https://doi.org/10.1167/jov.21.1.2

Benson, N. C., Kupers, E. R., Barbot, A., Carrasco, M., & Winawer, J. (2021). Cortical magnification in human visual cortex parallels task performance around the visual field. *eLife*, *10*. https://doi.org/10.7554/eLife.67685

Brainard, D. H. (1997). The psychophysics toolbox. *Spatial Vision*, *10*(4), 433-436.

Bruce, V., & Young, A. (1986). Understanding face recognition. *British Journal of Psychology*, *77(3)*, 305-327. https://doi.org/10.1111/j.2044-8295.1986.tb02199.x

Carrasco, M., Talgar, C. P., & Cameron, E. L. (2001). Characterizing visual performance fields: effects of transient covert attention, spatial frequency, eccentricity, task and set size. *Spatial Vision*, *15*(1), 61-75. https://doi.org/10.1163/15685680152692015

Cox, R. W. (1996). AFNI: software for analysis and visualization of functional magnetic resonance neuroimages. *Computers and Biomedical Research*, *29*(3), 162-173. https://doi.org/10.1006/cbmr.1996.0014

Dale, A. M., Fischl, B., & Sereno, M. I. (1999). Cortical surface-based analysis. I. Segmentation and surface reconstruction. *NeuroImage*, *9*(2), 179-194. https://doi.org/10.1006/nimg.1998.0395

de Haas, B., Schwarzkopf, D. S., Alvarez, I., Lawson, R. P., Henriksson, L., Kriegeskorte, N., & Rees, G. (2016). Perception and Processing of Faces in the Human Brain Is Tuned to Typical Feature Locations. *The Journal of Neuroscience*, *36*(36), 9289-9302. https://doi.org/10.1523/JNEUROSCI.4131-14.2016

DeYoe, E. A., Bandettini, P., Neitz, J., Miller, D., & Winans, P. (1994). Functional magnetic resonance imaging (FMRI) of the human brain. *Journal of Neuroscience Methods*, *54*(2), 171-187. https://doi.org/10.1016/0165-0270(94)90191-0

Dumoulin, S. O., & Wandell, B. A. (2008). Population receptive field estimates in human visual cortex. *NeuroImage*, *39*(2), 647-660. https://doi.org/10.1016/j.neuroimage.2007.09.034

Duncan, R. O., & Boynton, G. M. (2003). Cortical magnification within human primary visual cortex correlates with acuity thresholds. *Neuron*, *38*(4), 659-671. https://doi.org/10.1016/S0896-6273(03)00265-4

Engel, S. A., Glover, G. H., & Wandell, B. A. (1997). Retinotopic organisation in human visual cortex and the spatial precision of functional MRI. *Cerebral Cortex*, *7*, 181-192. https://doi.org/10.1093/cercor/7.2.181

Fang, F., Murray, S. O., & He, S. (2007). Duration-dependent FMRI adaptation and distributed viewer-centered face representation in human visual cortex. *Cerebral Cortex*, *17*(6), 1402-1411. https://doi.org/10.1093/cercor/bhl053

Finzi, D., Gomez, J., Nordt, M., Rezai, A. A., Poltoratski, S., & Grill-Spector, K. (2021). Differential spatial computations in ventral and lateral face-selective regions are scaffolded by structural connections. *Nature Communications*, *12*(1), 2278. https://doi.org/10.1038/s41467-021-22524-2

Fischl, B. (2012). FreeSurfer. *NeuroImage*, *62*(2), 774-781. https://doi.org/10.1016/j.neuroimage.2012.01.021

Fischl, B., Sereno, M. I., & Dale, A. M. (1999). Cortical surface-based analysis. II: Inflation, flattening, and a surface-based coordinate system. *NeuroImage*, *9*(2), 195-207. https://doi.org/10.1006/nimg.1998.0396

Fortenbaugh, F. C., Silver, M. A., & Robertson, L. C. (2015). Individual differences in visual field shape modulate the effects of attention on the lower visual field advantage in crowding. *Journal of Vision*, *15*(2), 19-19. https://doi.org/10.1167/15.2.19

Greenwood, J. A., Szinte, M., Sayim, B., & Cavanagh, P. (2017). Variations in crowding, saccadic precision, and spatial localization reveal the shared

topology of spatial vision. *Proceedings of the National Academy of Sciences*, *114*(17), E3573-E3582. https://doi.org/10.1073/pnas.1615504114

Grill-Spector, K., Weiner, K. S., Kay, K., & Gomez, J. (2017). The Functional Neuroanatomy of Human Face Perception. *Annual Review of Vision Science*, *3*, 167-196. https://doi.org/10.1146/annurev-vision-102016-061214

Groen, I. I. A., Dekker, T. M., Knapen, T., & Silson, E. H. (2022). Visuospatial coding as ubiquitous scaffolding for human cognition. *Trends in Cognitive Sciences*, *26*(1), 81-96. https://doi.org/10.1016/j.tics.2021.10.011

Henson, R. N. (2016). Repetition suppression to faces in the fusiform face area: A personal and dynamic journey. *Cortex*, *80*, 174-184. https://doi.org/10.1016/j.cortex.2015.09.012

Himmelberg, M. M., Tuncok, E., Gomez, J., Grill-Spector, K., Carrasco, M., & Winawer, J. (2023). Comparing retinotopic maps of children and adults reveals a late-stage change in how V1 samples the visual field. *Nature Communications*, *14*(1), 1561. https://doi.org/10.1038/s41467-023-37280-8

Himmelberg, M. M., Winawer, J., & Carrasco, M. (2020). Stimulus-dependent contrast sensitivity asymmetries around the visual field. *Journal of Vision*, *20*(9), 18. https://doi.org/10.1167/jov.20.9.18

Himmelberg, M. M., Winawer, J., & Carrasco, M. (2023). Polar angle asymmetries in visual perception and neural architecture. *Trends in Neurosciences*, *46*(6), 445-458. https://doi.org/10.1016/j.tins.2023.03.006

Hughes, A. E., Greenwood, J. A., Finlayson, N. J., & Schwarzkopf, D. S. (2019). Population receptive field estimates for motion-defined stimuli. *NeuroImage*, *199*, 245-260. https://doi.org/10.1016/j.neuroimage.2019.05.068

Kalpadakis-Smith, A. V., Goffaux, V., & Greenwood, J. A. (2018). Crowding for faces is determined by visual (not holistic) similarity: Evidence from judgements of eye position. *Scientific Reports*, *8*(1), 12556. https://doi.org/10.1038/s41598-018-30900-0

Kanwisher, N., McDermott, J., & Chun, M. M. (1997). The fusiform face area: a module in human extrastriate cortex specialized for face perception. *The Journal of Neuroscience*, *17*(11), 4302-4311. https://doi.org/10.1523/JNEUROSCI.17-11-04302.1997

Kay, K. N., Weiner, K. S., & Grill-Spector, K. (2015). Attention reduces spatial uncertainty in human ventral temporal cortex. *Current Biology*, *25*(5), 595-600. https://doi.org/10.1016/j.cub.2014.12.050

Kay, K. N., Winawer, J., Mezer, A., & Wandell, B. A. (2013). Compressive spatial summation in human visual cortex. *Journal of Neurophysiology*, *110*(2), 481-494. https://doi.org/10.1152/jn.00105.2013

Kleiner, M., Brainard, D., & Pelli, D. (2007). What's new in Psychtoolbox-3?

Kovacs, P., Knakker, B., Hermann, P., Kovacs, G., & Vidnyanszky, Z. (2017). Face inversion reveals holistic processing of peripheral faces. *Cortex*, *97*, 81-95. https://doi.org/10.1016/j.cortex.2017.09.020

Kurzawski, J. W., Burchell, A., Thapa, D., Majaj, N. J., Winawer, J. A., & Pelli, D. G. (2021). An enhanced Bouma model fits a hundred people's visual crowding. *bioRxiv*. https://doi.org/10.1101/2021.04.12.439570

Langner, O., Dotsch, R., Bijlstra, G., Wigboldus, D. H. J., Hawk, S. T., & van Knippenberg, A. (2010). Presentation and validation of the Radboud Faces Database. *Cognition & Emotion*, *24*(8), 1377-1388. https://doi.org/10.1080/02699930903485076

Le Grand, R., Mondloch, C. J., Maurer, D., & Brent, H. P. (2001). Early visual experience and face processing. *Nature*, *410*(6831), 890. https://doi.org/10.1038/35073749

Linhardt, D., Pawloff, M., Hummer, A., Woletz, M., Tik, M., Ritter, M., Schmidt-Erfurth, U., & Windischberger, C. (2021). Combining stimulus types for improved coverage in population receptive field mapping. *NeuroImage*, *238*, 118240. https://doi.org/10.1016/j.neuroimage.2021.118240

McKone, E. (2004). Isolating the special component of face recognition: peripheral identification and a Mooney face. *Journal of Experimental Psychology: Learning, Memory, and Cognition*, *30*(1), 181-197. https://doi.org/10.1037/0278-7393.30.1.181

Miller, K. D. (2016). Canonical computations of cerebral cortex. *Current Opinion in Neurobiology*, *37*, 75-84. https://doi.org/10.1016/j.conb.2016.01.008

Morsi, A. Y., Goffaux, V., & Greenwood, J. A. (2024). The resolution of face perception varies systematically across the visual field. *PloS One*, *19*(5), e0303400. https://doi.org/10.1371/journal.pone.0303400

Natu, V. S., Barnett, M. A., Hartley, J., Gomez, J., Stigliani, A., & Grill-Spector, K. (2016). Development of Neural Sensitivity to Face Identity Correlates with Perceptual Discriminability. *The Journal of Neuroscience*, *36*(42), 10893-10907. https://doi.org/10.1523/JNEUROSCI.1886-16.2016

Nelder, J. A., & Mead, R. (1965). A Simplex-Method for Function Minimization. *Computer Journal*, *7*(4), 308-313. https://doi.org/10.1093/comjnl/7.4.308

Pelli, D. G. (1997). The VideoToolbox software for visual psychophysics: Transforming numbers into movies. *Spatial Vision*, *10*, 437-442.

Poltoratski, S., Kay, K., Finzi, D., & Grill-Spector, K. (2021). Holistic face recognition is an emergent phenomenon of spatial processing in face-selective regions.

Nature Communications, *12*(1), 4745. https://doi.org/10.1038/s41467-021-24806-1

Quek, G. L., & Finkbeiner, M. (2014). Face-sex categorization is better above fixation than below: Evidence from the reach-to-touch paradigm. *Cognitive, Affective, & Behavioral Neuroscience*, *14*, 1407-1419. https://doi.org/10.3758/s13415-014-0282-y

Quek, G. L., & Finkbeiner, M. (2016). The upper-hemifield advantage for masked face processing: Not just an attentional bias. *Attention, Perception, & Psychophysics*, *78*, 52-68. https://doi.org/10.3758/s13414-015-0965-7

Rossion, B. (2008). Picture-plane inversion leads to qualitative changes of face perception. *Acta Psychologica*, *128*(2), 274-289. https://doi.org/10.1016/j.actpsy.2008.02.003

Rossion, B., & Gauthier, I. (2002). How does the brain process upright and inverted faces? *Behavioral and Cognitive Neuroscience Reviews*, *1*(1), 63-75. https://doi.org/10.1177/1534582302001001004

Roux-Sibilon, A., Peyrin, C., Greenwood, J. A., & Goffaux, V. (2023). Radial bias in face identification. *Proceedings of the Royal Society B: Biological Sciences*, *290*(2001), 20231118. https://doi.org/10.1098/rspb.2023.1118

Rubin, N., Nakayama, K., & Shapley, R. (1996). Enhanced perception of illusory contours in the lower versus upper visual hemifields. *Science*, *271*(5249), 651-653. https://doi.org/10.1126/science.271.5249.651

Schmidtmann, G., Logan, A. J., Kennedy, G. J., Gordon, G. E., & Loffler, G. (2015). Distinct lower visual field preference for object shape. *Journal of Vision*, *15*(5), 18. https://doi.org/10.1167/15.5.18

Schwarzkopf, D. S. (2022). SamSrf 9.4 - Matlab toolbox for pRF analysis. https://doi.org/10.17605/OSF.IO/2RGSM

Schwarzkopf, D. S., Anderson, E. J., de Haas, B., White, S. J., & Rees, G. (2014). Larger extrastriate population receptive fields in autism spectrum disorders. *The Journal of Neuroscience*, *34*(7), 2713-2724. https://doi.org/10.1523/JNEUROSCI.4416-13.2014

Sereno, M. I., Dale, A. M., Reppas, J. B., Kwong, K. K., Belliveau, J. W., Brady, T. J., Rosen, B. R., & Tootell, R. B. (1995). Borders of multiple visual areas in humans revealed by functional magnetic resonance imaging. *Science*, *268*(5212), 889-893. https://doi.org/10.1126/science.7754376

Silson, E. H., Groen, I. I. A., & Baker, C. I. (2022). Direct comparison of contralateral bias and face/scene selectivity in human occipitotemporal cortex. *Brain Structure and Function*, *227*(4), 1405-1421. https://doi.org/10.1007/s00429-021-02411-8

Silson, E. H., Reynolds, R. C., Kravitz, D. J., & Baker, C. I. (2018). Differential sampling of visual space in ventral and dorsal early visual cortex. *The Journal of Neuroscience*, *38*(9), 2294-2303. https://doi.org/10.1523/JNEUROSCI.2717-17.2018

Silva, M. F., Brascamp, J. W., Ferreira, S., Castelo-Branco, M., Dumoulin, S. O., & Harvey, B. M. (2018). Radial asymmetries in population receptive field size and cortical magnification factor in early visual cortex. *NeuroImage*, *167*, 41-52. https://doi.org/10.1016/j.neuroimage.2017.11.021

Silva, M. F., Harvey, B. M., Jorge, L., Canário, N., Machado, F., Soares, M., d'Almeida, O. C., & Castelo-Branco, M. (2021). Simultaneous changes in visual acuity, cortical population receptive field size, visual field map size, and retinal thickness in healthy human aging. *Brain Structure and Function*, *226*, 2839-2853. https://doi.org/10.1007/s00429-021-02338-0

Stigliani, A., Weiner, K. S., & Grill-Spector, K. (2015). Temporal Processing Capacity in High-Level Visual Cortex Is Domain Specific. *The Journal of Neuroscience*, *35*(36), 12412–12424. https://doi.org/10.1523/JNEUROSCI.4822-14.2015

Tanaka, K. (1996). Inferotemporal cortex and object vision. *Annual Review of Neuroscience*, *19*, 109-139. https://doi.org/10.1146/annurev.ne.19.030196.000545

van Dijk, J. A., de Haas, B., Moutsiana, C., & Schwarzkopf, D. S. (2016). Intersession reliability of population receptive field estimates. *NeuroImage*, *143*, 293-303. https://doi.org/10.1016/j.neuroimage.2016.09.013

Visconti di Oleggio Castello, M., Taylor, M., Cavanagh, P., & Gobbini, M. I. (2018). Idiosyncratic, Retinotopic Bias in Face Identification Modulated by Familiarity. *eNeuro*, *5*(5). https://doi.org/10.1523/ENEURO.0054-18.2018

Weiner, K. S., & Grill-Spector, K. (2010). Sparsely-distributed organization of face and limb activations in human ventral temporal cortex. *NeuroImage*, *52*(4), 1559-1573. https://doi.org/10.1016/j.neuroimage.2010.04.262

Westheimer, G. (2003). The distribution of preferred orientations in the peripheral visual field. *Vision Research*, *43*(1), 53-57. https://doi.org/10.1016/s0042-6989(02)00398-x

Witthoft, N., Poltoratski, S., Nguyen, M., Golarai, G., Liberman, A., LaRocque, K. F., Smith, M. E., & Grill-Spector, K. (2016). Reduced spatial integration in the ventral visual cortex underlies face recognition deficits in developmental prosopagnosia. *BioRxiv*, *051102*. https://doi.org/10.1101/051102

Yin, R. K. (1969). Looking at upside-down faces. *Journal of Experimental Psychology*, *81*(1), 141. https://doi.org/10.1037/h0027474